buildings

MDPI

Article

Bond Performance of Anti-Corrosion Bar Embedded in Ceramsite Concrete in Freeze–Thaw Cycles and Corrosive Environments

Yan Liu [1,2], Qiang Zhu [2], Jinhua Teng [2], Peng Deng [1,2,*] and Yan Sun [2]

[1] Shandong Provincial Key Laboratory of Civil Engineering Disaster Prevention and Mitigation, Shandong University of Science and Technology, Qingdao 266590, China
[2] College of Civil Engineering and Architecture, Shandong University of Science and Technology, Qingdao 266590, China
* Correspondence: dengpeng1226@sdust.edu.cn

Abstract: At present, basalt fiber-reinforced polymer (BFRP) bars and epoxy-coated steel reinforcing bars (ECRs) are very promising in ocean engineering. In this study, the bond strength degradation characteristics of BFRP bars, ECR, and ordinary steel bars (OSBs) embedded in ceramsite concrete (CC) were compared in a single-corrosive environment (acid, salt, and alkaline salt, respectively) coupled with freeze–thaw (FT) cycles (0, 15, or 30); a total of 111 specimens were designed. In the three corrosive environments, the BFRP-bar-CC specimens and OSB-CC specimens all failed to pull out, while the ECR-CC specimens showed splitting failure. When corrosive and FT cycles acted together, the failure modes of BFRP-bar-CC specimens and ECR-CC specimens did not change. However, when the FT cycles increased from 15 to 30, the type of failure for the OSB-CC specimens changed from pullout failure to splitting failure. In addition, the bonding strength of the three kinds of bars decayed most rapidly in an acid environment. When 30 FT cycles were applied, the bond strength of ECR-CC specimens and OSB-CC specimens decreased most rapidly in the acid environment, by 9.12% and 18.62%, respectively. However, the bond strength of BFRP-bar-CC decreased most rapidly, by 17.2%, in an alkaline salt environment.

Keywords: basalt fiber-reinforced polymer bars; bond strength; ceramsite concrete; corrosive environment; epoxy-coated steel bars; freeze–thaw cycle

Citation: Liu, Y.; Zhu, Q.; Teng, J.; Deng, P.; Sun, Y. Bond Performance of Anti-Corrosion Bar Embedded in Ceramsite Concrete in Freeze–Thaw Cycles and Corrosive Environments. *Buildings* **2023**, *13*, 884. https://doi.org/10.3390/buildings13040884

Academic Editors: Shan Gao, Jingxuan Wang, Dewen Kong and Yong Liu

Received: 9 March 2023
Revised: 26 March 2023
Accepted: 26 March 2023
Published: 28 March 2023

1. Introduction

In the main normative documents, such as ACI 318 [1], EN 1992 [2], and GB 50010-2010 [3], the properties of the bonding between the reinforcement and the surrounding concrete are crucial for the bearing capacity or safety performance of the reinforced concrete (RC) structure. Lightweight aggregate concrete (LWAC), especially ceramsite concrete (CC), can reduce the self-weight of reinforced concrete members. In addition, it possesses relatively good freeze–thaw (FT) resistance and realizes good heat insulation. Therefore, it holds promising prospects for application, particularly in cold or intensely corrosive ocean areas [4–6]. Although CC has good corrosion resistance, the weak corrosion resistance of steel bars affects bond performance [7]. As a result, numerous studies have focused on developing reasonable alternative materials for OSBs in order to elevate the bond performance of LWAC structures.

The use of stainless steel, fiber-reinforced polymers (FRPs), and epoxy-coated reinforcements (ECRs) is considered to be a good approach to addressing corrosion. However, the use of stainless-steel reinforcement is limited by its high cost [8]. Epoxy-coated reinforcement (ECR) has the advantages of low cost, corrosion resistance, and good ductility and durability [9–12]. However, the surface of ECR is easily damaged during construction [13]. Despite this defect, the engineering application of ECR has been gradually popularized;

thus, its bonding with CC requires our attention. In order to achieve better corrosion resistance, increasing attention has been paid to FRP in recent years.

Basalt FRP (BFRP) bars can be used as a suitable substitute for steel bars in reinforced concrete structures [14], due to their good chemical corrosion resistance, high fatigue resistance, thermal stability, and low water absorption [15–19]. The function of these excellent characteristics on the bond properties of FRP-reinforced concrete structures under FT conditions, cold regions, and ocean environments requires further study. Green et al. [20] introduced FT cycles to investigate the effect of FRP plates and concrete bonding properties, revealing that, with failure, the surface turned into an adhesive interface with the FRP plates with an increasing number of cycles. In contrast, in the absence of FT cycles, failure occurs on concrete substrates, which makes the bond strength of FRP bars controlled not by concrete strength but by interlaminar shear strength beneath the resin layer of reinforcement [21,22]. Shi et al. [23] reported that the durability of BFRP composites was largely maintained in an FT environment. Firas et al. [24] conducted a supplementary experiment to simulate the marine environment by soaking samples in brine; the results showed that when the bearing capacity decreased by 48%, the resin–concrete interface was damaged. FRP is exposed to one or more aging media during its service life, such as FT cycles, acid rain, or marine erosion. Therefore, the durability of FRP in corrosive environments remains a problem [25]. For instance, Hassan M et al. [26], Yan et al. [27], Wu et al. [28], and Mohamed Al et al. [29] confirmed that an alkaline solution (attempting to simulate concrete-pore solutions) was the main influencing condition for BFRP bars. Altalmas et al. [30] studied the bond durability of BFRP in different corrosive environments (acid, salt, or alkali). It was found that the bond strength of BFRP specimens decreased by 25% after 90 days of immersion in seawater and alkaline solutions, and decreased by 14% when they were immersed in an acidic solution for 90 days.

Many previous studies only investigated the bonding properties between bars (BFRP bars, ECRs) and ordinary Portland cement (OPC), but few of them studied reinforcement with CC, and even fewer studied the bonding properties in harsh environments. This study evaluated the decay of the bond strength of BFRP bars under corrosive conditions. The combined effects of FT cycling and corrosion conditions were evaluated and compared with their effects on ECRs and OSBs. The failure mechanism of the specimens was analyzed and the bond–slip relationship was proposed.

2. Materials and Methods

2.1. Specimen Size and Structure

A total of 111 specimens were prepared, including 81 central pullout cube specimens with a side length of 150 mm and 30 compressive strength cube specimens with a side length of 100 mm. The 150 mm concrete cubes were concentrically reinforced with 330 mm of BFRP, ECR, and ordinary steel bar (OSB), and the BFRP and ECR were compared with the OSB. According to ACI440.3R-04 [31], the embedding length was 5 d [32] (Figure 1a), where d is the diameter of the ECR. In order to increase the required bonding length, the PVC sleeve is set at the loading end position of each specimen, and the gap between the PVC sleeve and the steel bar is filled and sealed with a foaming agent to prevent its grouting from affecting the test results. The samples were cured in a curing chamber with 95% relative humidity at ambient temperature (20 $\pm$ 2 °C) for 28 days. (Figure 1b). The cured specimens were subjected to the FT cycle test and corrosion solution test, respectively.

2.2. Raw Materials

2.2.1. Concrete

Lightweight aggregate (LWA) uses shale ceramic products produced by Yichang Huiteng Ceramic Products Trading Co., Ltd., Yichang, China. Table 1 shows the characteristic parameters of shale ceramsite (SC). Table 2 shows the proportions of CC used to cast the specimens. The cement is made of 42.5 OPC, the fine aggregate is made of natural medium sand with a fineness coefficient of 2.6, and the coarse aggregate is made of SC with

a maximum particle size of 20 mm. Tap water was used. In order to improve the fluidity of the cement mixture, Grey Ba brand high-efficiency water-reducing agent was added to the test at a dosage of 0.1~0.3%. The concrete compressive strengths were determined using 100 × 100 × 100 mm cube specimens. The 28-day compressive strengths are listed in Table 3.

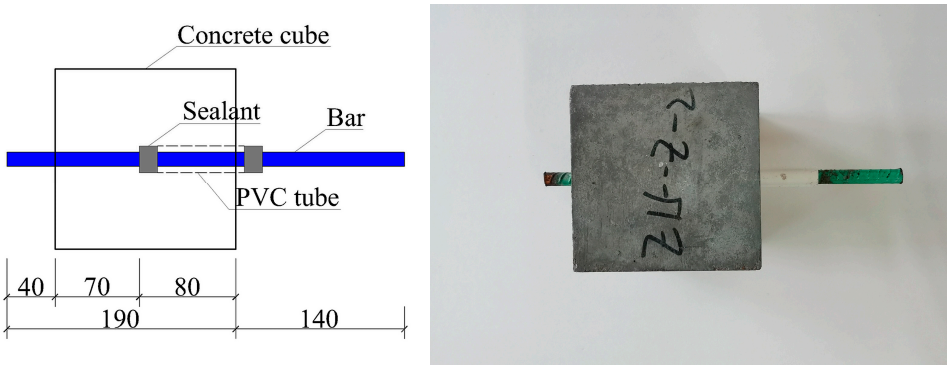

(**a**) (**b**)

Figure 1. Pullout samples. (**a**) Schematic diagram of the bond test sample (mm); (**b**) sample of concrete after curing.

Table 1. Characteristic parameters of shale ceramsite (SC).

Ceramsite Type	Density Grad (kg/m^3)	Nominal Diameter (mm)	Packing Density (kg/m^3)	Water Absorption 1 h (%)	Compressive Strength (MPa)
SC	500	5–20	470	7.6	2.6

Table 2. Mixture ratio of CC.

Compressive Strength	Cement (kg/m^3)	Water (kg/m^3)	Fine Aggregate (kg/m^3)	Coarse Aggregate (kg/m^3)
LC30 *	400	200	680	490

* LC30, the compressive strength of CC after 28 days of curing is close to 30 MPa.

Table 3. The measured values of concrete strength.

Compressive Strength	Measured Compressive Strength (MPa)			Mean (MPa)
	1	2	3	
LC30	34.56	33.58	31.48	33.21

2.2.2. Bars

The diameter and length of the three reinforcing bars were 14 mm and 330 mm, respectively (Figure 2). BFRP bars were customized by Jingdong Construction Technology Co., Ltd., Shanghai, China. A pultrusion process was used to combine basalt fibers with epoxy resins. The fiber-to-epoxy volumetric ratios were 65% and 35%, respectively, and the BFRP bars met the minimum requirements of ACI440.3R-04 [31] and CSAS807 [33]. The epoxy coated steel bar was customized by Deyang Wanteng Metal Products Co., Ltd., Deyang, China, the coating thickness was 0.17 mm, the main raw materials of epoxy coating included epoxy resin, curing agent, and additives. The tensile properties of the reinforcement test are shown in Table 4. BFRP is not suitable for reinforcing flexural members due to its low elastic modulus, as it will lead to excessive deflection and cracking of the reinforced members.

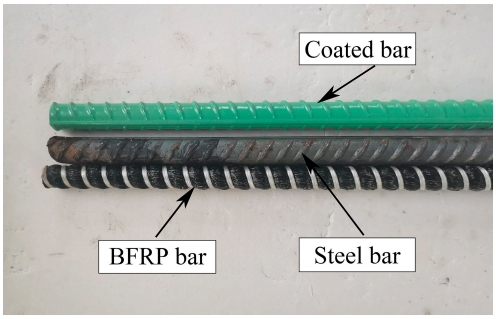

Figure 2. Bar types.

Table 4. Mechanical properties of bars.

Bar Type	Diameter (mm)	Ultimate Tensile Strength (MPa)	Yield Strength (MPa)	Elastic Modulus (GPa)
BFRP bars	14	703	-	40
ECRs	14	660	470	208
OSBs	14	655	566	202

2.3. Experimental Scheme

2.3.1. Bond Specimens and Concrete Test Cube

In this study, a series of experiments were designed to evaluate the influence of different factors on bond strength. The specific test groups are shown in Table 5. These variables were the type of reinforcement, FT cycles, the corrosive environment, and CC compressive strength. All bond specimens were labeled in the following order: bar type (basalt, B; epoxy-coated rebar, E; or ordinary steel bar, D), middle numbers indicating FT environment (0, 15, or 30) experienced by the specimen, and corrosive exposure (S for acid, Z for salt, and J for alkaline salt). For example, B-0-S is a specimen of BFRP bars and CC under a single acidic condition. The compressive strength samples were labeled in the following order: number of FT (0, 15, 30), conditional exposure (S for acid, Z for salt, and J for alkaline salt). For instance, 15-S is the specimen of CC under the combined action of 15 FT cycles and an acid environment.

Table 5. Testing plan.

Grouping	Specimens	Bar Type	FT Cycles	Corrosive Environment	Number of Specimens
Group 1 *	B-0-S/J/Z	BFRP	0	pH = 2/10/7	3/3/3
Group 2	E-0-S/J/Z	ECR	0	pH = 2/10/7	3/3/3
Group 3	D-0-S/J/Z	OSB	0	pH = 2/10/7	3/3/3
Group 4	B-15-S/J/Z	BFRP	15	pH = 2/10/7	3/3/3
Group 5	E-15-S/J/Z	ECR	15	pH = 2/10/7	3/3/3
Group 6	D-15-S/J/Z	OSB	15	pH = 2/10/7	3/3/3
Group 7	B-30-S/J/Z	BFRP	30	pH = 2/10/7	3/3/3
Group 8	E-30-S/J/Z	ECR	30	pH = 2/10/7	3/3/3
Group 9	D-30-S/J/Z	OSB	30	pH = 2/10/7	3/3/3
Group 10	-	-	Untreated specimen		3
Group11	0-S/J/Z	-	0	pH = 2/10/7	3/3/3
Group12	15-S/J/Z	-	15	pH = 2/10/7	3/3/3
Group13	30-S/J/Z	-	30	pH = 2/10/7	3/3/3

* Three corrosive environments were set up for each group of specimens: S/J/Z represent acid/alkaline salt/salt and pH of 2/10/7, respectively.

2.3.2. FT Cycles

The FT cabinet (NJW-HDK-5) was used for the accelerated aging test of the samples. Temperature monitoring was carried out by temperature-sensitive elements placed in the center and diagonal of the instrument.

FT cycle test scheme was based on ASTMC666/C666M [34]. The highest temperature of the FT test was set at 6 ± 2 °C, and the lowest temperature was −18 ± 2 °C. Before the FT test, the specimens, after curing for 24 days, were immersed in water at 20 ± 2 °C for 4 days. After soaking, the specimens were taken out and exposed to sunlight for 2 days to remove excess moisture.

2.3.3. Three Different Corrosive Solutions

Three artificial corrosive environments were used in this study: (1) an alkaline salt environment of pH 10, using a $NaHCO_3$ solution to simulate the alkaline environment in ordinary reinforced concrete; (2) a salt environment of pH 7, using a NaCl solution with a chloride concentration of 3.5% to simulate the climate of coastal areas; (3) an acid solution of pH 2.0, using an oxalic acid solution to simulate a polluted industrial area. After the FT cycles test, the specimens were immersed in the three solutions, respectively. There were three specimens in each solution, all of which were soaked for 60 days. The pH value of the three corrosive environments was monitored in real-time by a pH meter, and the corresponding solution was added in time to ensure that the pH was unchanged.

2.4. Pullout Test Scheme

The center pullout test was performed according to RILEM-FIP-CEB [35]. MTS-SANS series universal testing machine. A range of 400 kN was used for the single-end drawing of the specimen (Figure 3a,b). The displacement meter used epoxy resin glue to paste an angle steel bar horizontally on the free end of the steel bar, and the concrete surface, ensuring that the tie rod of the displacement meter and the angle steel surface were always at 90 degrees. LVDT1 was used to record the slip of the unloaded end rod, whereas LVDT2 recorded the slippage of the free end on the concrete surface. The displacement control was loaded at a rate of 0.2 mm/min. When the free-end slip reached 10 mm, all tests were halted unless the specimen failed before then (split failure).

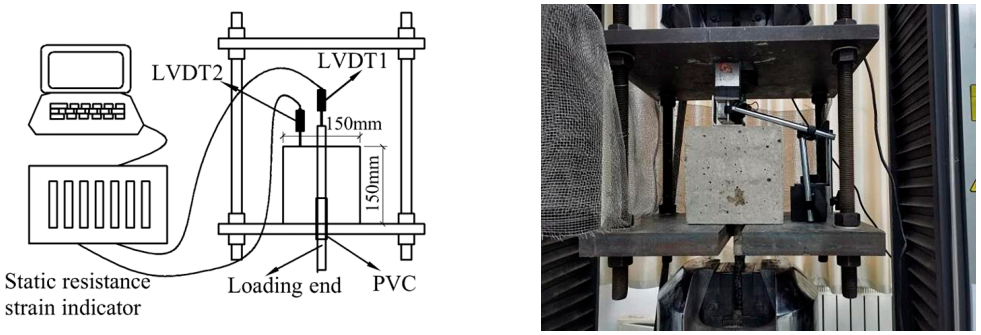

Figure 3. Pullout test setup. (**a**) Pullout test equipment; (**b**) universal tensile-compression testing machine.

3. Test Results and Discussion

3.1. The Bond Stress

Due to the low elastic modulus of BFRP bars, their elastic deformation cannot be ignored. The elastic elongation of BFRP bars can be obtained using Equation (1) [36]:

$$\delta_e = \frac{P}{EA}L \quad (1)$$

where δ_e is the elastic elongation of unbonded BFRP bars under drawing force, E is the elastic modulus of BFRP bars, A is the section area of BFRP bars, and L is the length of the bonding section.

The slip is then subtracted from the elastic elongation of the BFRP bar to obtain the true slip. This can be expressed as Equation (2) [37,38]:

$$s = s_m - \delta_e \quad (2)$$

where s is the real slip, and s_m is the slip amount of the BFRP bar measured by the displacement sensor.

The average bond stress between the bar and CC can be expressed as Equation (3) [39]:

$$\tau = \frac{P}{\pi d l_a} \quad (3)$$

where τ is the average bond stress (MPa), P is the pullout force of the bar (N), d is the diameter of the bar (mm), and l_a is the bond length of the bar (mm).

Table 6 shows the results of the drawing test. To ensure the reliability of the test results, three samples were tested in each group, and the final test result was the average value of the data of the three specimens.

Table 6. Bond test results of BFRP, ECR, and OSB specimens exposed to different environments.

Specimen	Failure Mode	P (kN)			$\overline{P}$ (kN) [3]	τ_{max} (MPa) [4]	S (mm)			$\overline{S}$ (mm) [5]
		1	2	3			1	2	3	
B-0-S	PO [1]	29.01	28.52	27.49	28.34	9.24	1.33	1.30	1.24	1.29
B-0-J	PO	28.43	28.02	29.68	28.71	9.45	1.20	1.16	1.27	1.21
B-0-Z	PO	28.34	28.90	/ [6]	28.62	9.42	1.13	1.25	/	1.19
E-0-S	S [2]	37.86	35.53	36.94	36.77	11.95	1.08	1.15	0.93	1.05
E-0-J	S	38.79	36.43	39.53	38.25	12.59	1.04	0.88	0.99	0.97
E-0-Z	S	35.23	40.49	39.30	38.34	12.52	0.79	1.12	0.85	0.92
D-0-S	PO	/	36.32	39.68	38.00	12.35	/	0.77	0.95	0.86
D-0-J	PO	39.69	40.39	39.95	40.01	13.17	0.86	0.90	0.73	0.83
D-0-Z	PO	37.60	42.60	39.38	39.86	13.12	0.70	0.94	0.79	0.81
B-15-S	PO	25.52	27.77	30.02	27.77	9.03	1.21	1.31	1.53	1.35
B-15-J	PO	25.76	26.05	29.01	26.94	8.76	1.30	1.27	1.36	1.31
B-15-Z	PO	28.54	29.62	27.67	28.61	9.30	1.20	1.38	1.17	1.25
E-15-S	S	33.27	37.64	32.59	34.50	11.55	1.11	1.17	0.99	1.09
E-15-J	S	40.61	37.26	35.26	37.71	12.26	1.03	0.78	0.74	0.85
E-15-Z	S	36.91	38.51	/	37.71	12.26	0.89	1.05	/	0.97
D-15-S	PO	31.60	33.82	37.51	34.31	11.15	0.80	0.80	0.95	0.85
D-15-J	PO	40.35	39.50	37.63	39.16	12.73	0.88	0.67	0.67	0.74
D-15-Z	PO	39.75	35.32	41.39	38.82	12.62	0.54	0.66	0.57	0.59
B-30-S	PO	25.67	26.03	28.73	26.81	8.71	1.79	1.87	2.01	1.89
B-30-J	PO	23.38	/	24.76	24.07	7.82	1.63	/	1.55	1.59
B-30-Z	PO	27.19	26.59	29.32	27.70	9.00	1.49	1.34	1.61	1.48
E-30-S	S	34.81	31.59	33.83	33.41	10.86	1.39	1.09	1.27	1.25
E-30-J	S	38.77	33.83	36.96	36.52	11.87	1.04	0.86	1.07	0.99
E-30-Z	S	37.96	33.12	38.36	36.48	11.86	0.80	0.67	0.90	0.79
D-30-S	S	29.86	31.96	/	30.91	10.05	1.15	1.01	/	1.08
D-30-J	S	38.40	36.24	39.12	37.92	12.32	1.02	0.79	0.92	0.91
D-30-Z	S	39.37	38.21	36.09	37.89	12.31	0.81	0.62	0.52	0.65

[1] PO, pullout failure; [2] S, splitting failure; [3] $\overline{P}$, mean value of ultimate load; [4] τ_{max}, maximum bond strength; [5] $\overline{S}$, mean free end slip; [6] /, the sample value exceeds the value specified in the specification and is not accepted.

3.2. Concrete Compressive Strength

Table 7 shows the change in compressive strength of untreated specimens and specimens in three corrosive environments. The compressive strength in alkaline and salt environments was similar to that of non-corroded specimens, which was similar to previous studies [30]. However, the compressive strength of concrete immersed in an acid solution decreased significantly due to acid erosion. Compared with the alkaline salt environment and the salt environment, the acid environment had the greatest influence on the compressive strength of the CC specimen.

Table 7. Compressive strength of concrete after corrosion and FT.

Grouping	Specimen	$f_{c,pH}$ (MPa) [1]			$\overline{f}_{c,pH}$ (MPa) [2]
		1	2	3	
Group 10	Untreated specimen	34.56	33.58	31.48	33.21
Group 11	0-S	28.41	28.72	28.22	28.45
	0-J	34.22	33.41	32.62	33.42
	0-Z	31.51	32.56	34.63	32.90
Group 12	15-S	22.02	21.76	21.09	21.62
	15-J	16.90	26.75	28.90	26.75
	15-Z	28.04	26.53	25.35	26.64
Group 13	30-S	18.26	18.32	17.62	18.07
	30-J	25.17	20.92	22.43	22.84
	30-Z	21.96	21.53	22.92	22.14

[1] $f_{c,pH}$, compressive strength (MPa); [2] $\overline{f}_{c,pH}$, the average compressive strength (MPa).

3.3. Failure Mode

Table 6 shows the failure models of all the specimens. It can be seen that the BFRP-bar-CC specimens all experienced pullout failure, but all the ECR-CC specimens failed in splitting. The failure mode of the OSB-CC specimens was the most notable. Under three single-corrosive environments, it experienced pullout failure. However, under the combined action of FT and corrosion, the pullout failure became a splitting failure as the FT number increased from 15 to 30. The failure mode of this specimen was mainly divided into two types: steel bar pullout failure and concrete splitting failure. In the pullout failure, when the loading starts, the displacement at both ends of the sample was very small. When the tension gradually rose to 70–90% of the peak load, a significant displacement of the steel bar could be observed at the free end. Although the splitting failure of concrete is a result of brittleness, there is no obvious sign before the splitting failure occurs. When the drawing force reached the ultimate load, the damage occurred suddenly, accompanied by a loud sound, and the specimen was broken into two or three segments.

In order to analyze the failure mode of specimens more carefully, we studied typical specimens in three corrosive environments (e.g., B-0-S, D-0-Z, E-0-S, E-0-Z, E-0-J) and typical specimens under the combined action of corrosive environments and FT cycles (e.g., E-30-J, B-30-J, D-15-J, D-30-J).

3.3.1. Specimens in Corrosive Environments

Figure 4 shows the failure phenomena of typical specimens in three corrosive environments. After the test, the samples were segmented to observe the condition of the reinforcement and concrete in the embedded area. The BFRP-bar-CC specimens all failed to pull out in three kinds of corrosive environments, which was due to the corrosion resistance of epoxy resin-based grease on the surface of BFRP bars. We were able to observe that the surface of BFRP bars was smooth and did not change significantly in the corrosive environment (Figure 4a). The OSB-CC specimens also failed to pull out in three kinds of corrosive environments. When we cut the specimen open, we were able to observe that the surface of the rib material was slightly corroded (Figure 4b). However, all the ECR-CC specimens experience splitting failure because the outer protective layer effectively resisted the erosion of the acid, alkali, and salt environments. In the acid environment, a layer of white mesh material was attached to the inner reinforcement surface of CC, and the rib surface fell off (Figure 4c). In the salt environment, the surface of ECR was slightly peeled off (Figure 4d). In the alkaline salt environment, the surface coating clearly fell off and adhered to the CC (Figure 4e).

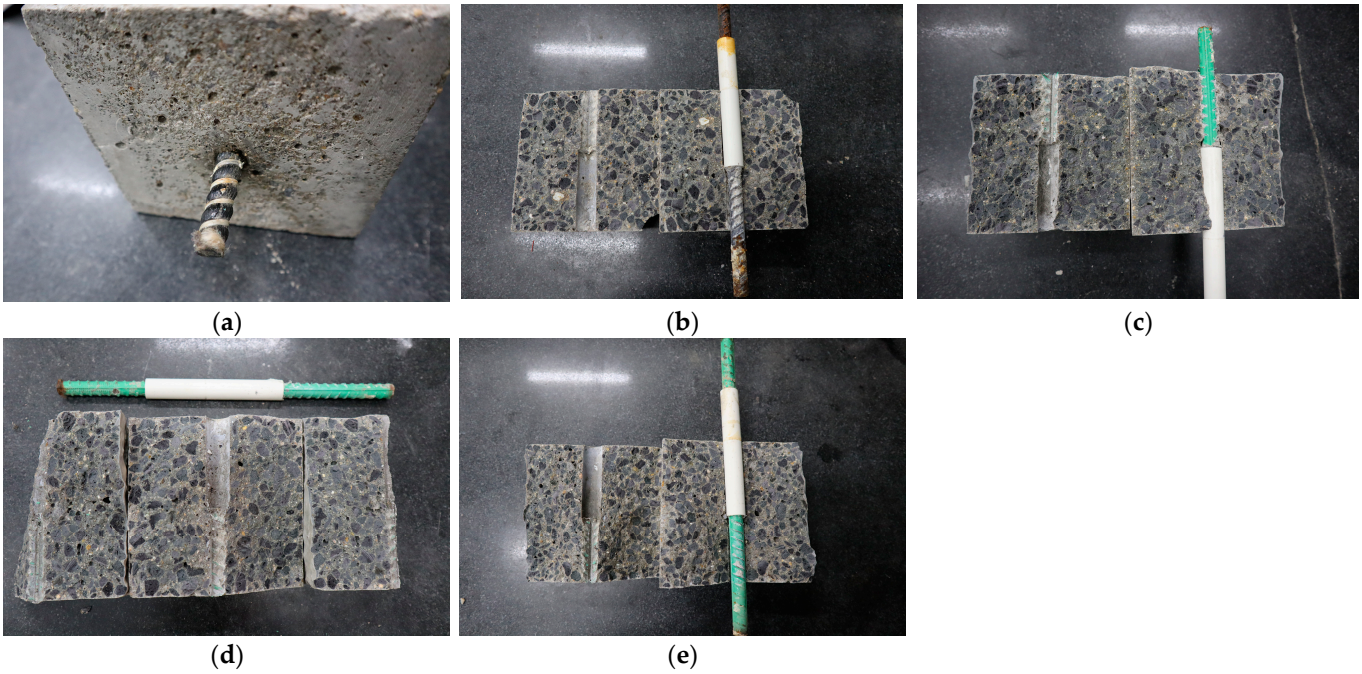

Figure 4. Typical failure modes for samples after a corrosive environment. (**a**) B-0-S; (**b**) D-0-S; (**c**) E-0-S; (**d**) E-0-Z; (**e**) E-0-J.

3.3.2. Specimens in FT Cycles and Corrosive Environments

It can be seen from Table 6 that the combination of FT cycles and corrosive environments had a more significant effect on the bond strength of specimens than the single corrosive environment. The failure mode of part of the bar-CC bond specimen is shown in Figure 5. The ECR-CC experienced splitting failure due to the high force required to pull the coated rebar out of the CC. In the alkaline salt corrosion environment, the coating on the surface of the coated steel rib fell off (Figure 5a), white reactants were formed between the reinforcement and CC, and an epoxy coating was attached to the CC. Under the coupled action of FT cycling and a corrosive environment, the BFRP-bar-CC specimens all failed to pull out. After the interaction of 30 FT cycles (FT30) and an alkaline salt environment (Figure 5b), the surface strands of BFRP bars fell off, and the surface became significantly rough. Under the action of 15 FT cycles (FT15) and a corrosive environment, the OSB specimens were mostly pulled out, the steel bars were gradually pulled out from the loading end of the specimen, and no cracks were observed on the surface of the specimen (Figure 5c). However, under the coupling effect of FT30 and a corrosive environment, the common ribbed-steel specimen largely failed by splitting, and the concrete broke into two or three segments. Due to the sudden failure, the crack length and width were large, and a loud sound occurred during the failure (Figure 5d).

3.4. Weight Loss

Due to the FT cycles and the corrosive environments, concrete surface spalling occurred. Generally speaking, the quality of concrete has a certain relationship with its surface state. Especially in FT cycle environments, spalling usually starts locally and expands to a larger area or even the entire concrete surface. Finally, the surface of the sample will appear uneven or aggregate exposure may occur [27,40]. Equation (4) is used to analyze the weight loss of all specimens after erosion:

$$\Delta W_n = \frac{W_0 - W_r}{W_r} \times 100\% \quad (4)$$

where ΔW_n is the weight loss of CC specimens after environmental erosion, W_0 is the weight of the sample before it erodes the environment, and W_r is the weight of the corroded sample.

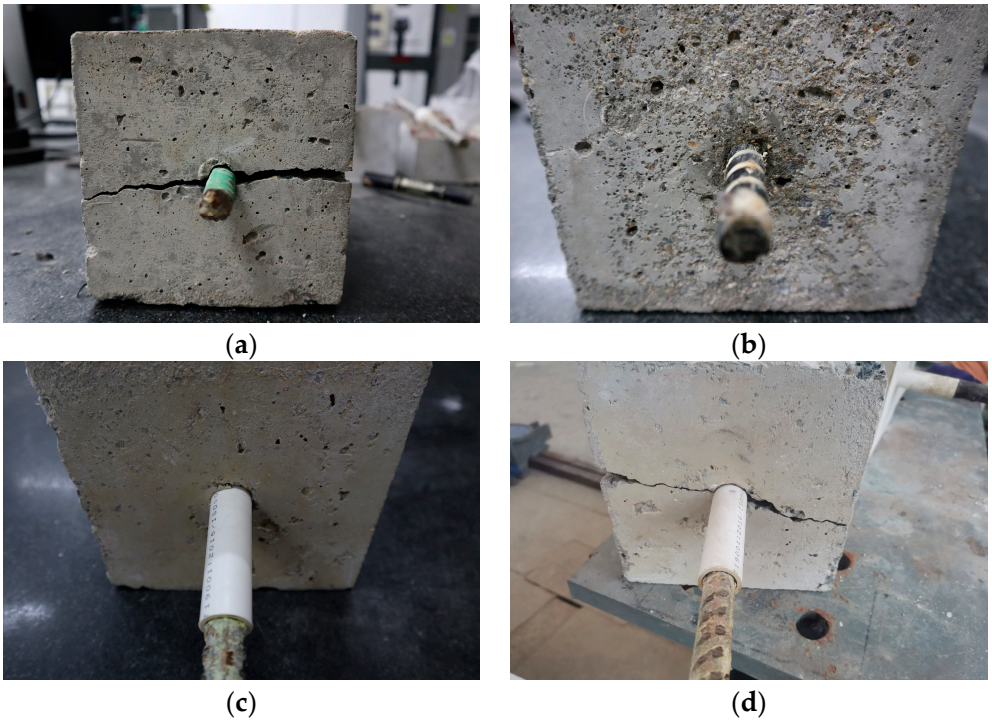

Figure 5. Typical failure modes for samples after the corrosive environment and FT cycles. (**a**) E-30-J; (**b**) B-30-J; (**c**) D-15-J; (**d**) D-30-J.

As can be seen from Table 8 and Figure 6, for the specimens that were exposed to single-corrosive environments, the weight-loss rate of CC specimens exposed to the alkaline salt environment and the salt environment was similar: 0.18% and 0.12%, respectively. The weight loss rate of CC exposed to acid was 0.24%. This shows that acid corrosive solution can peel off the surface cementitious material of concrete [41]. In addition, it can be seen from Table 8 that when FT cycles are not considered, the influence of the three corrosive environments on CC specimens was smaller than the coupling effect of the FT cycles and corrosive environments. However, when the specimens underwent the coupling effect of FT30 and a corrosive environment, the weight-loss rate of the specimens increased to 1.85% (acid environment), 1.64% (alkaline salt environment), and 1.65% (salt environment). It can be seen that the weight-loss rate of specimens subjected to the coupled effect of FT cycles and corrosive environments was significantly higher than that of specimens subjected to a single factor.

Table 8. Weight loss of CC samples undergoing FT environment and corrosive environment.

Specimen	W_0 (g)			W_r (g)			ΔW_n (%)			Mean (%)
	1	2	3	1	2	3	1	2	3	
0-S	1749	1698	1704	1745	1694	1700	0.23	0.24	0.24	0.24
0-J	1681	1704	1662	1678	1698	1654	0.18	0.19	0.18	0.18
0-Z	1648	1668	1645	1646	1668	1643	0.12	0.00	0.12	0.12
15-S	1664	1709	1737	1649	1693	1721	0.91	0.95	0.93	0.93
15-J	1632	1651	1671	1619	1638	1656	0.80	0.79	0.91	0.83
15-Z	1636	1623	1677	1620	1609	1665	0.83	0.87	0.72	0.81
30-S	1656	1657	1705	1626	1627	1674	1.85	1.84	1.85	1.85
30-J	1712	1640	1740	1685	1613	1712	1.60	1.67	1.64	1.64
30-Z	1695	1775	1647	1668	1746	1620	1.62	1.66	1.67	1.65

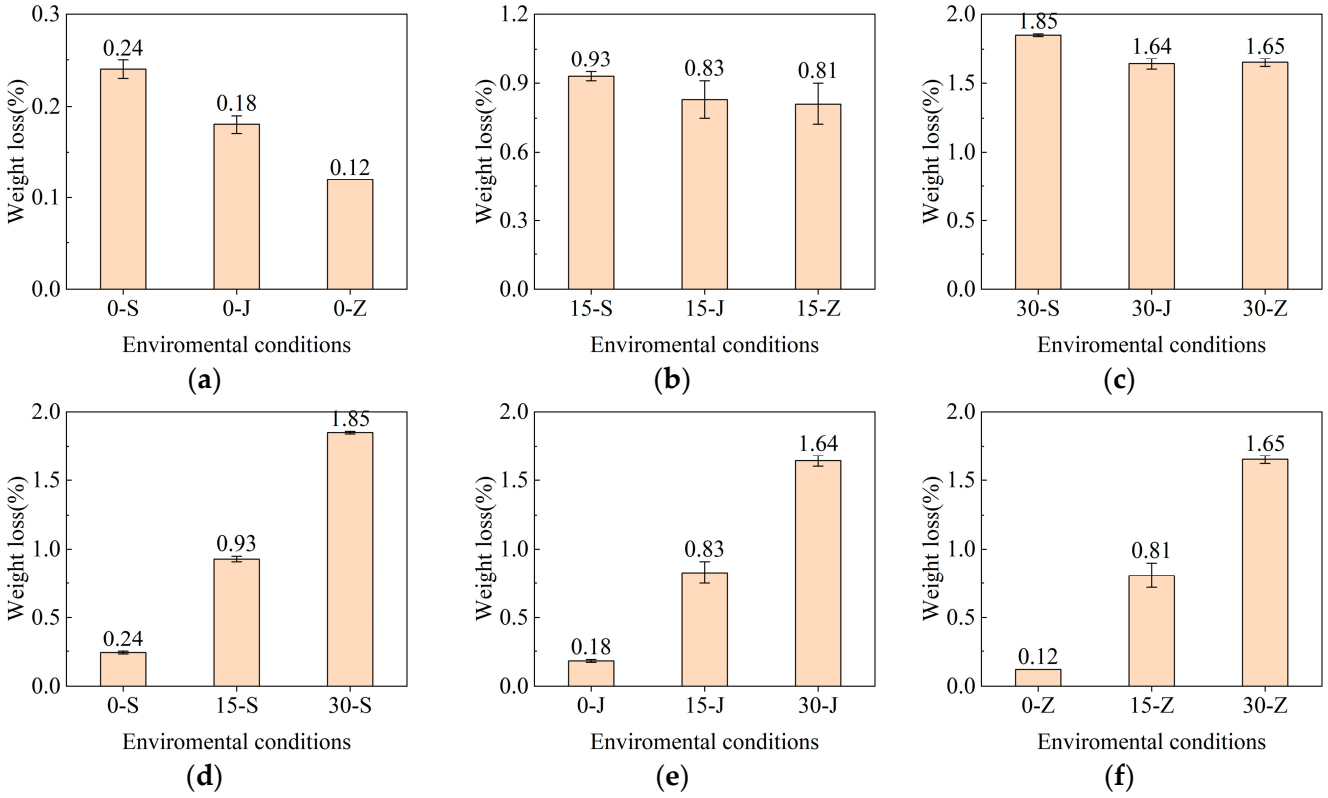

Figure 6. Mass loss in different corrosive environments and FT environments. (**a**) Different corrosive environments; (**b**) 15 FT cycles and different corrosive environments; (**c**) 30 FT cycles and different corrosive environments; (**d**) different FT cycles and the acid environment; (**e**) different FT cycles and the alkaline salt environment; (**f**) different FT cycles and the salt environment.

3.5. Bond Stress–Slip Curves

Figure 7 shows the bond stress–slip curves of three types of reinforcement in different corrosive environments. Each specimen's bond performance was slightly different in different corrosive environments. Among them, we can see that the τ_{max} is the lowest in the acid environment. Kong and Orbison [42] found that the strength of concrete decreased gradually under acidic conditions (pH 2), which was about 70% of the 28-day age strength of uncorroded concrete specimens. For BFRP bar-CC specimens, the τ_{max} (9.45 MPa) in an alkaline salt environment was only 0.3% higher than that under a salt environment (9.42 MPa). In an acid environment, the τ_{max} of BFRP-bar-CC specimens was 9.24 MPa, which is 2.2% lower than that in an alkaline salt environment. For OSB specimens, the τ_{max} of acid (12.35 MPa) was 6.2% lower than that of alkaline salt (13.17 MPa). In the acid environment, the τ_{max} of ECR–CC specimens was 11.95 MPa, which was 3.2% lower than that of OSB-CC specimens. To sum up, the τ_{max} of the same reinforced specimen in an alkaline salt environment, a salt environment, and the acid environment went from higher to lower in a single-corrosive environment.

As shown in Figure 8, the bond–slip curves of all the specimens present obvious upward trends before failure. However, the samples that experienced splitting failure (e.g., E-15-S) belong to the brittle failure category, and the bond–slip curve showed no downward trend. When exposed to 30 FT cycles under the corrosive conditions of an acid environment or salt environment, the bond strength loss of the BFRP bar-CC specimens were similar: 3.3% and 4.4%, respectively. When the corrosive environment was alkaline salt and the number of FT cycles was increased from 15 to 30 times, it could be observed that the τ_{max} of the BFRP-bar-CC specimen was reduced by about 10.66%, from 8.76 MPa to 7.82 MPa. The results show that in the same corrosive environment, the bond strength of the specimen decreased and the slip increased with an increase in the number of FT cycles.

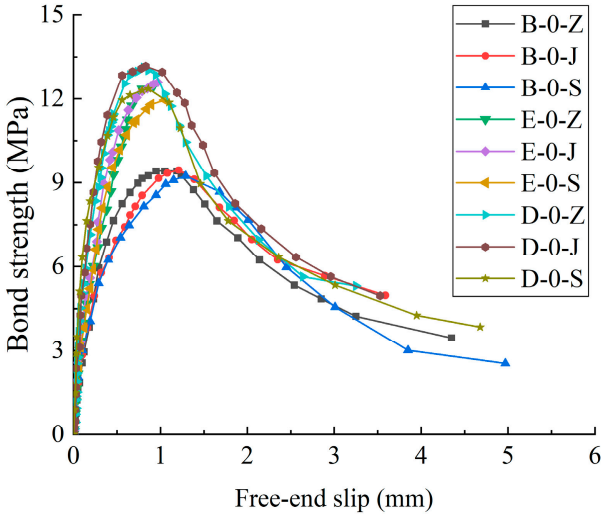

Figure 7. Bond stress–slip curves at the free end for BFRP bar specimens, ECR specimens, and OSB specimens in different corrosive environments.

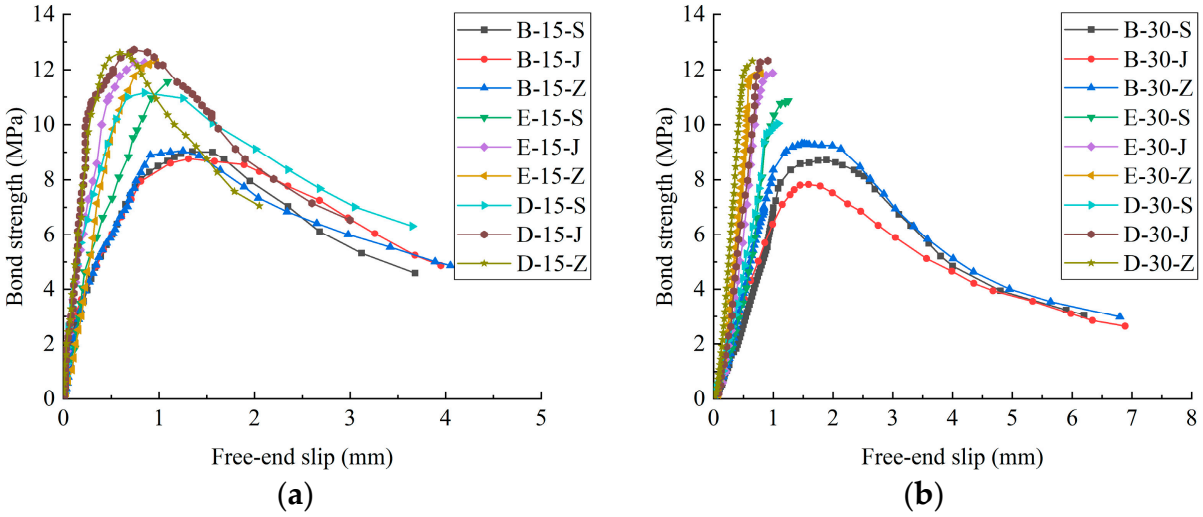

Figure 8. Bond stress–slip curves at the free end for BFRP bar specimens, ECR specimens, and OSB specimens under the combined action of FT cycles and corrosive environments. (**a**) 15 FT cycles and corrosive environments; (**b**) 30 FT cycles and corrosive environments.

In the same environmental conditions, the correspondence of τ_{max} with different reinforcement specimens was quite different. Taking the coupling effect of the acid environment and FT30 as an example, the $\overline{S}$ corresponding to the τ_{max} of the BFRP-bar–CC specimen was 1.89 mm, that of ECR-CC was 1.25 mm, and that of the OSB-CC specimen was the smallest, that is 1.08 mm. It can be seen that BFRP bars and ECRs showed a high slippage due to the smooth epoxy resin-based grease coating.

3.6. Analysis of Influence Factors of Bond Strength

Bank et al. [43] found a correlation between the degradation of fibrous materials and the reduction of bond strength. As can be seen in Figure 9c, under the combined action of FT30 and an alkaline salt environment, the τ_{max} of the three reinforcement materials, in descending order, were: OSB, ECR, and BFRP bar. We can see that the τ_{max} of BFRP bar specimen is always the lowest, and the reason is that there is a layer of epoxy resin on the surface of the bar. The analysis of the τ_{max} of these three kinds of steel bars shows that under the coupled effect of FT30 and an alkaline salt environment, the τ_{max} of ECR is 3.7% lower than that of OSB, and the τ_{max} of BFRP bar is 36.52% lower than that of OSB.

However, under the coupled effect of FT30 and an acid environment, the τ_{max} of OSB is 7.47% lower than that of ECR, and the τ_{max} of BFRP bar is 19.47% lower than that of ECR.

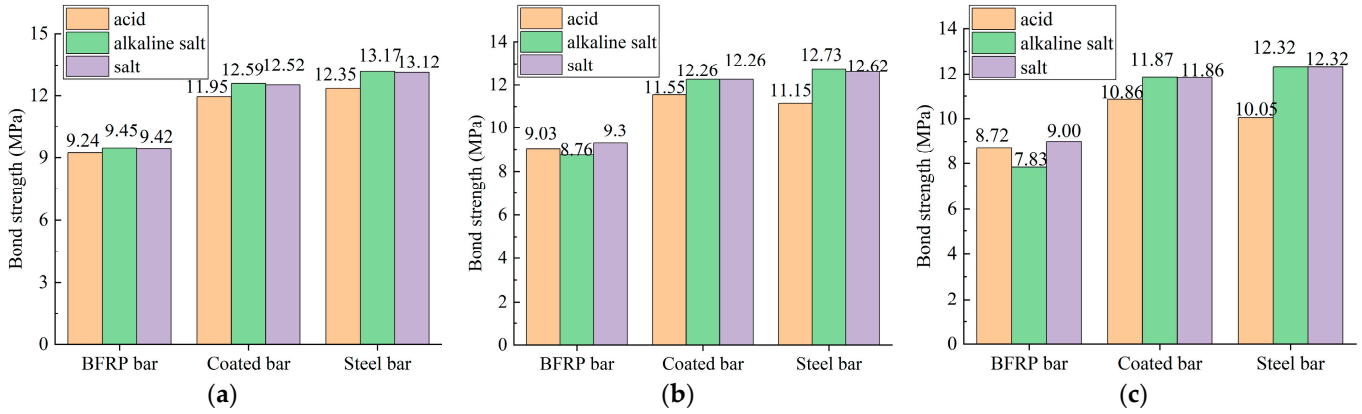

Figure 9. The influence of different factors on bonding performance. (**a**) Single corrosive environment; (**b**) FT15 + corrosive environment; (**c**) FT30 + corrosive environment.

It can be seen from Figure 9c that the τ_{max} of ECR in an alkaline salt environment is similar to that in a salt environment: both were about 11.80 MPa. The τ_{max} of the specimen in the acid environment was the lowest (10.86 MPa), which was 8.43% lower than that in the salt environment. In addition, it can be seen that the bond strength of ECRs and OSBs immersed in the alkaline and salt environments was greater than that of the specimens exposed to an acid environment. This is due to the high alkalinity and moisture of the internal environment of the concrete, with a pH of 10.5 to 13.5 [44]. The chloride in the water erodes the concrete, forming chemicals that can be absorbed and expanded, thus damaging the concrete [45–47]. In this case, while the strength of concrete decreases, the bond strength of the specimen in the acid environment decreases.

4. Calibration of Bonding Models to FT Cycles and Corrosive Environments

In this study, the bond properties of reinforced concrete under drawing loads were analyzed by using existing models. Xu et al. [48] studied the influence of various factors on the bond strength of ordinary crescent steel. However, they did not consider the influence of FT cycle times (N) and corrosive environments (pH).

$$\tau_{max} = \left(0.82 + 0.9\frac{d}{l_a}\right)\left(1.6 + 0.7\frac{c}{d}\right)f_t \quad (5)$$

where d is the diameter of reinforcement material, l_a is the bond strength, c is the thickness of CC protective layer, f_t is the splitting tensile strength of CC, and N is the FT cycle number and the pH of the corrosive solution.

Wang Peng et al. [49] studied the relationship between splitting tensile strength and compressive strength and proposed Equation (6).

$$f_{t,0} = 0.33 f_{c,0}^{\frac{2}{3}} \quad (6)$$

Based on Equations (5) and (6), the type of reinforcement material, diameter of reinforcement material d, bond length L_a, thickness of protective layer c, splitting tensile strength f_t, number of FT cycles N, and the pH of the corrosive solution, the ultimate bond strength of different reinforcement materials and CC under the combined action of FT cycle and corrosive environment is established, as shown in Equation (7):

$$\tau_{max} = \left(a_0 + a_1 \times N + a_2 \times \mathrm{pH} + a_3 \times \frac{d}{L_a}\right)\left(a_4 \times N + a_5 \times \mathrm{pH} + a_6 \times \frac{c}{d}\right) \times f_t \quad (7)$$

Origin 2018 was subsequently used to fit Formula (7) and to obtain Formulas (8)–(10), and each parameter was obtained. For BFRP-reinforced concrete calibration, the parameters a_0, a_1, a_2, a_3, a_4, a_5, and a_6 were 0.5, −0.0126, −0.0565, 7.2611, 0.0342, 0.0417, and 0.3162, respectively. Similarly, ECR concrete calibration parameters a_0, a_1, a_2, a_3, a_4, a_5, and a_6 were 0.7, −0.0297, 0.00182, −12.19, 0.0138, 0.0155, and −0.4676, respectively. OSB concrete calibration parameters a_0, a_1, a_2, a_3, a_4, a_5, and a_6 were 0.65, −0.0257, 0.0486, −14.3947, 0.0110, −0.0391, and −0.3702, respectively. These parameters are closely related to the bond stress and the corresponding slip.

According to Equations (6) and (7), we can calculate the ultimate bond strength of BFRP-bar-CC specimens, ECR-CC specimens, and OSB-CC specimens using Equations (8)–(10):

$$\tau_{\max,B} = \left(0.5 - 0.0126N - 0.0565\text{pH} + 7.2611\frac{d}{l_a}\right)\left(0.0342N + 0.0417\text{pH} + 0.3162\frac{c}{d}\right) \times f_t \quad (8)$$

$$\tau_{\max,E} = \left(0.7 - 0.0297N + 0.00182\text{pH} + 12.19\frac{d}{l_a}\right)\left(0.0138N + 0.0155\text{pH} - 0.4676\frac{c}{d}\right) \times f_t \quad (9)$$

$$\tau_{\max,D} = \left(0.65 - 0.0257N + 0.0486\text{pH} - 14.3947\frac{d}{l_a}\right)\left(0.011N - 0.0391\text{pH} - 0.3702\frac{c}{d}\right) \times f_t \quad (10)$$

In this paper, the ultimate bond strength calculated according to the formula of the bond strength is compared with the ultimate bond strength obtained by a test, and the results are shown in Figure 10. In order to further analyze the degree of coincidence between the calculated value and the test value, the root-mean-square error was used. The closer the root mean square error value is to zero, the higher the degree of coincidence. For the BFRP bar, ECR, and OSB, the root-mean-square error formula produced values of 0.148, 0.124, and 0.137, respectively. As can be seen from the figure, the fitting results are in good agreement with the experimental results.

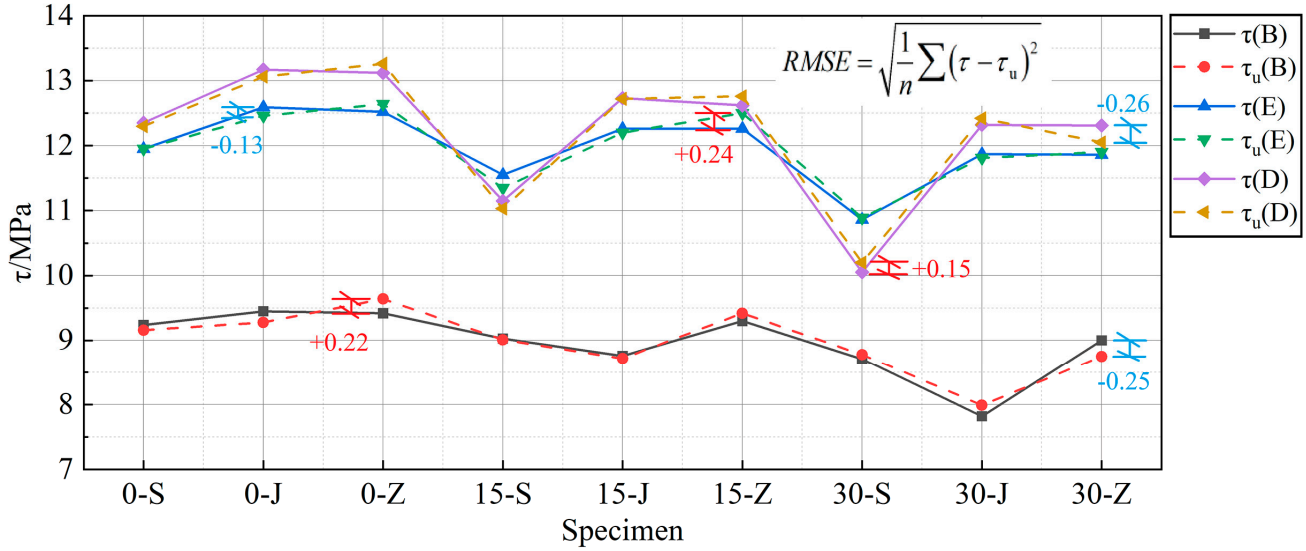

Figure 10. Comparison between the calculated values τ_u and experimental values τ of ultimate bond stress.

5. Conclusions

In this paper, by analyzing the influence of single corrosion environment (acid, alkali, alkaline salt) and the coupling effect of corrosion and FT cycle (0, 15, 30) on the bond strength attenuation of three bar-CC specimens (BFRP-bar-CC, OSB-CC, ECR-CC), the following conclusions were reached:

1. In three corrosive environments, the failure mode of BFRP-bar-CC specimens and OSB-CC specimens was a pullout failure, while the failure mode of ECR-CC specimens

was a split failure. When FT and corrosion acted together, the failure mode of BFRP-bar-CC specimens and ECR-CC specimens did not change, while the failure mode of OSB-CC specimens changed from a pullout failure to a splitting failure as the number of FT cycles increased from 15 to 30;

2. For the same bar-CC specimens, different corrosive environments had a slight influence on the bonding property of the specimens. For BFRP-bar-CC specimens, the most rapid decline of bond strength was observed in an acid environment. Compared with an acid environment, the bond strength in an alkaline salt environment and a salt environment increased by 2.2% and 1.9%, respectively;
3. When exposed to the coupled effect of an acid environment and 30 FT cycles, the bond strength of BFRP-bar-CC specimens, OSB-CC specimens, and ECR-CC specimens were decreased 5.7%, 18.6%, and 9.12%, respectively. This indicates that the BFRP-bar-CC specimens possessed good acid corrosion resistance, which can effectively prevent bond strength reduction;
4. When exposed to the coupled effect of 30 FT cycles and a corrosive environment, BFRP-CC specimens showed the most rapid decline (17.2%) in an alkaline environment, while OSB-CC specimens and ECR-CC specimens showed the most rapid degradation (18.6% and 9.12%, respectively) in an acid environment;
5. The formulas for calculating the ultimate bond strength of BFRP bars, ECRS, and OSBS with CC under the combined action of FT cycles and corrosive environments are provided. The obtained results are in good agreement with the experimental results.

Author Contributions: Conceptualization, Y.L. and Q.Z.; methodology, Q.Z.; formal analysis, Q.Z. and J.T.; investigation, J.T. and Y.S.; resources, Y.L. data curation, Y.L. and J.T.; writing—original draft preparation, Q.Z.; writing—review and editing, Y.L. and J.T.; visualization, Q.Z. and J.T.; supervision, Y.L. and P.D.; project administration, P.D. All authors have read and agreed to the published version of the manuscript.

Funding: This research received no external funding.

Data Availability Statement: The data presented in this study are available on request from the corresponding author.

Conflicts of Interest: The authors declare no conflict of interest.

References

1. *ACI 318*; Building Code Requirements for Structural Concrete (ACI 318-08) and Commentary (ACI 318R-08). American Concrete Institute: Farmington Hills, MI, USA, 2009.
2. *EN 1992*; Eurocode 2: Design of Concrete Structures—Part 1-1: General Rules and Rules for Buildings. European Committee for Standardization (CEN): Brussels, Belgium, 2014.
3. *GB 50010-2010*; Code for Design of Concrete Structures. China Architecture & Building Press: Beijing, China, 2015.
4. Mehany, S.; Mohamed, H.M.; Benmokrane, B. Contribution of lightweight self-consolidated concrete (LWSCC) to shear strength of beams reinforced with basalt FRP bars. *Eng. Struct.* **2021**, *231*, 111758. [CrossRef]
5. Ji, T.; Zheng, D.; Chen, X.; Lin, X.; Wu, H. Effect of prewetting degree of ceramsite on the early-age autogenous shrinkage of lightweight aggregate concrete. *Constr. Build. Mater.* **2015**, *98*, 102–111. [CrossRef]
6. Tanyildizi, H.; Coskun, A. The effect of high temperature on compressive strength and splitting tensile strength of structural lightweight concrete containing fly ash. *Constr. Build. Mater.* **2008**, *22*, 2269–2275. [CrossRef]
7. Fu, X.; Chung, D. Effect of corrosion on the bond between concrete and steel rebar. *Cem. Concr. Res.* **1997**, *27*, 1811–1815. [CrossRef]
8. Bautista, A.; Blanco, G.; Velasco, F. Corrosion behaviour of low-nickel austenitic stainless steels reinforcements: A comparative study in simulated pore solutions. *Cem. Concr. Res.* **2006**, *36*, 1922–1930. [CrossRef]
9. Nie, R.; Huang, Y.; Li, X.; Sun, H.; Li, D. Bond of epoxy-coated reinforcement to seawater coral aggregate concrete. *Ocean Eng.* **2020**, *208*, 107350. [CrossRef]
10. McDonald, D.B.; Pfeifer, D.W.; Sherman, M.R. Corrosion evaluation of epoxy-coated, metallic-clad and solid metallic reinforcing bars in concrete. *Aust. Civ. Eng. Trans.* **2002**, *44*, 103–107.
11. Huang, Y.; Qi, X.; Li, C.; Gao, P.; Wang, Z.; Ying, J. Seismic behaviour of seawater coral aggregate concrete columns reinforced with epoxy-coated bars. *Structures* **2022**, *36*, 822–836. [CrossRef]

12. Gerardo, G.C. *Resistances of a Stainless Steel-Clad Reinforcing Bar to Chloride-Induce Corrosion in Concrete*; Virginia Transportation Research Council: Charlottesville, VA, USA, 2004.
13. Wang, J.; Gong, J.; Gong, Z.; Yang, X.; Wang, B. Effect of curing agent polarity on water absorption and free volume in epoxy resin studied by PALS. *Nucl. Instrum. Methods Phys. Res. Sect. B Beam Interact. Mater. At.* **2010**, *268*, 2355–2361. [CrossRef]
14. Sagar, B.; Sivakumar, M.V.N. Performance evaluation of basalt fibre-reinforced polymer rebars in structural concrete members—A review. *Innov. Infrastruct. Solut.* **2021**, *6*, 75. [CrossRef]
15. Lopresto, V.; Leone, C.; De Iorio, I. Mechanical characterisation of basalt fibre reinforced plastic. *Compos. Part B Eng.* **2011**, *4*, 717–723. [CrossRef]
16. Lapko, A.; Urbanski, M. Experimental and theoretical analysis of deflections of concrete beams reinforced with basalt rebar. *Arch. Civ. Mech. Eng.* **2015**, *15*, 223–230. [CrossRef]
17. Wang, X.; Wu, G.; Wu, Z.; Dong, Z.; Xie, Q. Evaluation of prestressed basalt fiber and hybrid fiber reinforced polymer tendons under marine environment. *Mater. Des.* **2014**, *64*, 721–728. [CrossRef]
18. Garcia-Espinel, J.D.; Castro-Fresno, D.; Gayo, P.P.; Ballester-Munoz, F. Effects of sea water environment on glass fiber reinforced plastic materials used for marine civil engineering constructions. *Mater. Des.* **2015**, *66*, 46–50. [CrossRef]
19. Borrie, D.; Liu, H.B.; Zhao, X.L.; Singh, R.R.K.; Bai, Y. Bond durability of fatigued CFRP-steel double-lap joints preexposed to marine environment. *Compos. Struct.* **2015**, *131*, 799–809. [CrossRef]
20. Mark, F.G.; Luke, A.B.; Yves, B. Effect of freeze–thaw cycles on the bond durability between fibre reinforced polymer plate reinforcement and concrete. *Can. J. Civ. Eng.* **2000**, *27*, 949–959. [CrossRef]
21. Achillides, Z.; Pilakoutas, K. Bond Behavior of Fiber Reinforced Polymer Bars under Direct Pullout Conditions. *J. Compos. Constr.* **2005**, *8*, 173–181. [CrossRef]
22. Refai, A.; Ammar, M. Bond Performance of Basalt Fiber-Reinforced Polymer Bars to Concrete. *J. Compos. Constr.* **2015**, *19*, 1–12. [CrossRef]
23. Shi, J.; Zhu, H.; Wu, Z. Bond Behavior between Basalt Fiber–Reinforced Polymer Sheet and Concrete Substrate under the Coupled Effects of Freeze-Thaw Cycling and Sustained Load. *J. Compos. Constr.* **2013**, *17*, 530–542. [CrossRef]
24. Firas, A.; Jean-Michel, M.; Mohamed, S. Bond strength of different strengthening systems-Concrete elements under freeze-thaw cycles and salt water immersion exposure. *Constr. Build. Mater.* **2014**, *70*, 399–409. [CrossRef]
25. Dong, Z.Q.; Wu, G. Research progress on durability of FRP bars reinforced concrete structures. *China Civ. Eng. J.* **2019**, *52*, 1–19. [CrossRef]
26. Hassan, M.; Benmokrane, B.; ElSafty, A. Bond durability of basalt-fiber-reinforced-polymer (BFRP) bars embedded in concrete in aggressive environments. *Compos. Part B Eng.* **2016**, *106*, 262–272. [CrossRef]
27. Fei, Y.; Zhibin, L.; Dalu, Z. Experimental study on bond durability of glass fiber reinforced polymer bars in concrete exposed to harsh environmental agents: Freeze-thaw cycles and alkaline-saline solution. *Compos. Part B Eng.* **2017**, *116*, 406–421. [CrossRef]
28. Wu, G.; Dong, Z.Q.; Wang, X.; Zhu, Y. Prediction of long-term performance and durability of BFRP bars under the combined effect of sustained load and corrosive solutions. *J. Compos. Constr.* **2015**, *19*, 04014058. [CrossRef]
29. Rifai, M.A.; El-Hassan, H.; El-Maaddawy, T. Durability of basalt FRP reinforcing bars in alkaline solution and moist concrete environments. *Constr. Build. Mater.* **2020**, *243*, 118258. [CrossRef]
30. Altalmas, A.; Refai, A.; Abed, F. Bond degradation of basalt fiber-reinforced polymer (BFRP) bars exposed to accelerated aging conditions. *Constr. Build. Mater.* **2015**, *81*, 162–171. [CrossRef]
31. *ACI 440.6M-08*; Guide Test Methods for Fiber-Reinforced Polymer (FRP) Composites for Reinforcing or Strengthening Concrete and Masonry Structures. American Concrete Institute: Farmington Hills, MI, USA, 2004.
32. Lu, Z.; Su, L.; Lai, J.; Xie, J.; Yuan, B. Bond durability of BFRP bars embedded in concrete with fly ash in aggressive environments. *Compos. Struct.* **2021**, *271*, 114121. [CrossRef]
33. *CAN/CSA S807e10 (R2015)*; Specification for Fiber Reinforced Polymers. Canadian Standards Association: Rexdale, ON, Canada, 2015.
34. *ASTM C666/C666M*; Standard Test Method for Resistance of Concrete to Rapid Freezing and Thawing. American Society for Testing and Materials: West Conshohocken, PA, USA, 2015.
35. Rilem, F.C. Tentative recommendations, recommendations for reinforcing steel, bond test for reinforcing steel: 1-Beam test (7-II-28 d) 2-pull-out test (7-II-128). *Mater. Struct.* **1973**, *6*, 79–118.
36. Amini, K.; Jalalpour, M.; Delatte, N. Advancing concrete strength prediction using non-destructive testing: Development and verification of a generalizable model. Constr. *Build. Mater.* **2016**, *102*, 762–768. [CrossRef]
37. Institute of Building Structure and Chinese Academy of Building Sciences. *Research and Application of Lightweight Aggregate Concrete*; China Architecture & Building Press: Beijing, China, 1981.
38. Deng, P.; Cong, Z.R.; Liu, Y.; Huang, Y.Y.; Zhu, Q. Effect of Dry-Wet Cycles on BFRP Bars and Modified Ceramsite Concrete in Marine Environments. *J. Mater. Civ. Eng.* **2022**, *34*, 040221251–0402212512. [CrossRef]
39. Shang, H.S.; Zhao, T.J.; Cao, W.Q. Bond behavior between steel bar and recycled aggregate concrete after freeze–thaw cycles. *Cold Reg. Sci. Technol.* **2015**, *118*, 38–44. [CrossRef]
40. Deng, P.; Wang, Y.J.; Sun, Y.; Liu, Y.; Guo, W.H. Bond durability of basalt-fiber-reinforced-polymer bars embedded in lightweight aggregate concrete subjected to freeze–thaw cycles. *Struct. Concr.* **2021**, *22*, 2829–2848. [CrossRef]

41. Wang, H.Z. An Experimental Study on the Deterioration of Properties of Fiber–Reinforced Concrete in Acid Corrosive Environments. Master's Thesis, Zhejiang University of Technology, Hangzhou, China, 2018.
42. Kong, H.L.; Orbison, J.G. Concrete deterioration due to acid precipitation. *ACI Mater. J.* **1987**, *84*, 110–115. [CrossRef]
43. Bank, L.C.; Puterman, M.; Katz, A. Effect of material degradation on bond properties of fiber reinforced plastic reinforcing bars in concrete. *ACI Mater. J.* **1998**, *95*, 232–243.
44. Barneyback, R.S.; Diamond, S. Expression and analysis of pore fluids from hardened cement pastes and mortars. *Cem. Concr. Res.* **1981**, *11*, 279–285. [CrossRef]
45. Fang, C.Q.; Karin, L.G.; Chen, L.G. Corrosion influence on bond in reinforced concrete. *Cem. Concr. Res.* **2004**, *10*, 2159–2167. [CrossRef]
46. Lee, S.T. Performance Deterioration of Portland Cement Matrix due to Magnesium Sulfate Attack. *KSCE J. Civ. Eng.* **2007**, *11*, 157–163. [CrossRef]
47. Lee, S.T.; Kim, D.G. Sulfate Attack of Cement Matrix Containing Inorganic Alkali-free Accelerator. *KSCE J. Civ. Eng.* **2009**, *13*, 49–54. [CrossRef]
48. Xun, Y.L.; Liu, L.X.; Guan, P.W.; Zeng, D.G. Anchorage Performance and Design Method of Epoxy Resin Coated Steel Bar. *Port Waterw. Eng.* **1999**, *8*, 33–37. [CrossRef]
49. Wang, P. Experimental Research on the Fundamental Mechanical Behavior of Ceramisite Concrete. Master's Thesis, Changsha University of Science & Technology, Changsha, China, 2008. [CrossRef]